Turbulent Boundary-Layer Properties Downstream of the Shock-Wave / Boundary-Layer Interaction

D. W. Kuntz*
Sandia National Laboratories, Albuquerque, New Mexico
V. A. Amatucci† and A. L. Addy‡
University of Illinois at Urbana-Champaign, Urbana, Illinois

An experimental investigation was conducted to study the interaction between a shock wave and a turbulent boundary layer. Compression corner models mounted on a wind tunnel floor were used to generate the oblique shock wave in the Mach 2.94 flowfield. Ramp angles of 8, 12, 16, 20, and 24 deg were used to produce the full range of possible flowfields, including flow with no separation, flow with incipient separation, and flow with a significant amount of separation. The principal measurement technique used was laser Doppler velocimetry (LDV), which was used to make two-component coincident velocity measurements within the redeveloping boundary layer downstream of the interaction. The results of the LDV measurements indicated that the boundary layer was significantly altered by the interaction. The mean streamwise velocity profiles downstream of the separated compression corners were very wake-like in nature, and the boundary-layer profiles downstream of all the interactions showed an acceleration of the flow nearest the wall as the boundary layers began to return to equilibrium conditions. Significant increases in turbulence intensities and Reynolds stresses were caused by the interactions, and indications of the presence of large-scale turbulent structures were obtained in the redeveloping boundary layers.

Nomenclature

C_f = skin friction coefficient
M = Mach number
P = pressure
Re_δ = Reynolds number based on boundary-layer thickness
u = mean velocity component parallel to the wind tunnel floor or ramp surface
u_τ = friction velocity, $(\tau_w/\rho_w)^{1/2}$
u^* = Van Driest generalized velocity
v = mean velocity component perpendicular to the wind-tunnel floor or ramp surface
X = longitudinal coordinate
X^+ = longitudinal coordinate parallel to the ramp surface
Y = vertical coordinate
Y^* = displaced vertical coordinate
α = ramp angle
δ = boundary-layer thickness
δ^* = boundary-layer displacement thickness, $\delta^* = \int_0^\delta (1 - \rho u/\rho_e u_e)\,dY$
δ_0 = undisturbed boundary-layer thickness at $X = 0$
θ = boundary-layer momentum thickness, $\theta = \int_0^\delta [\rho u/\rho_e u_e](1 - u/u_e)\,dY$
ν = kinematic viscosity
Π = wake strength parameter
ρ = density
τ = shear stress
$\langle\ \rangle$ = root-mean-square quantity

Subscripts

e = boundary-layer edge
MAX = maximum
R = reattachment
S = separation
w = wall
∞ = freestream condition, upstream of the shock wave

Superscripts

$\bar{(\ )}$ = ensemble average
$(\ )'$ = fluctuation from the mean value

Presented as Paper 86-0348 at the AIAA 24th Aerospace Sciences Meeting, Reno, NV, Jan. 6–9, 1986; received March 18, 1986; revision received Aug. 27, 1986.

*Member of Technical Staff, Aerothermodynamics Division. Member AIAA.
†Graduate Research Assistant, Department of Mechanical and Industrial Engineering. Student Member AIAA.
‡Professor and Associate Head, Department of Mechanical and Industrial Engineering. Associate Fellow AIAA.

Introduction

THE interaction between a shock wave and a turbulent boundary layer has been a topic of interest to researchers for many years. Flowfields of this type occur frequently in high-speed flight, and a thorough knowledge of the effects of the shock wave on the boundary-layer properties is necessary for accurate flowfield prediction. The investigation described in this report was conducted in order to provide detailed mean and turbulent flowfield properties within boundary layers downstream of shock-wave/turbulent-boundary-layer interactions of various strengths.

A review of the literature published in this area indicates that there is a need for additional measurements within shock-wave/boundary-layer interaction flowfields.[1] A great deal of effort has been dedicated to determining mean properties within these flowfields,[2-5] and some investigations have measured turbulent flowfield properties.[6-12] Unfortunately, the few investigations which have used hot-wire or laser Doppler velocimeter (LDV) systems to study these flowfields have been limited to single-component measurements, and thus have presented a rather limited amount of information. The numerical simulations of these flowfields have achieved some degree of success, but shortcomings exist in the available turbulence models. Advances in turbulence modeling await a better understanding of the nature of turbulence itself. The current investigation was conducted with a two-component

LDV system, and thus has produced new information concerning the nature of the turbulence downstream of the shock-wave/turbulent-boundary-layer interaction.

Compression corner models, or ramps mounted on the wind tunnel floor, were used to generate the oblique shock waves for this study. Ramp angles of 8, 12, 16, 20, and 24 deg were used to produce the full range of possible flowfields, including flow with no separation, flow with incipient separation, and flow with a significant amount of separation. In this manner, the effects of increasing shock strength on the turbulent properties of the boundary layer were studied systematically.

Measurement techniques used in this investigation included schlieren photography, surface static pressure measurement, surface streak pattern measurement, and laser Doppler velocimetry. The LDV system was used to make two-component coincident velocity measurements within the upstream boundary layer and within the redeveloping boundary layers downstream of the interactions. The two-component nature of the LDV system allowed direct measurement of the two instantaneous velocity components. These data then enabled calculation of the two mean velocity components, as well as various turbulent properties, such as turbulence intensities, Reynolds stress, turbulence structure parameters, skewness and flatness factors, and turbulence triple products. Space limitations prevent the presentation of all the data obtained, but a complete presentation of these data can be found in Ref. 1. The purpose of this paper is to present an overview of the data obtained in this investigation, with specific emphasis on the effects of increasing shock strength on the various flowfield parameters.

Experimental Facilities

The experiments described in this paper were conducted in the Mechanical Engineering Laboratory of the University of Illinois at Urbana-Champaign. The wind tunnel used in this investigation operated in the blow-down mode and had a 10.2×10.2 cm test section. A solid aluminum nozzle produced a Mach number of 2.94 within the test section. Transparent windows within the wind tunnel sidewalls provided the optical access necessary for schlieren photography and laser Doppler velocimetry. Additional details of the wind tunnel facility can be found in Ref. 1.

The data of this investigation were obtained with a wind-tunnel stagnation pressure of approximately 483 kPa (70 psia). This pressure level was high enough to ensure proper supersonic operation of the wind tunnel, yet was low enough to permit relatively long run times of approximately 90 s. The stagnation temperature was near the ambient temperature in the laboratory facility, and thus the wind tunnel operated with nearly adiabatic conditions within the wall boundary layers.

A diagram of a typical compression corner model is shown in Fig. 1 with the coordinate system used in the presentation of the experimental data. A complete compression corner model consisted of a ramp mounted on a ramp support. The forward part of the ramp support formed the lower wind-tunnel wall upstream of the corner. The section of the model downstream of the end of the ramp sloped gradually down to the floor level of the wind tunnel to reduce the disturbances caused by the models during the wind-tunnel startup process.

The five ramp models and the ramp support were made of aluminum and anodized flat black to reduce laser light reflections during the LDV measurements. The model support was sealed along the sidewalls and upstream of the corner where the support mated with the wind-tunnel floor with linear O-ring material. The junction between the ramp and the ramp support which formed the compression corner was sealed with gasket-sealing compound. Static pressure taps 0.57 mm in diameter were located every 2.54 mm longitudinally on the surface of the ramps and on the model support upstream of the corner.

The models used in this study spanned the full 10.2-cm width of the test section. It may have proven beneficial to have used narrower ramp models with splitter plates located along the sides to eliminate the effects of the sidewall boundary layers on the shock-wave/boundary-layer interaction, similar to those used in other studies.[2-9] However, the sidewall splitter plates would have denied optical access to the interaction region, and thus would have made LDV measurements impossible. As a result, it was decided to use full span models and to experimentally determine the extent of the sidewall boundary-layer interference using surface flow pattern measurements.

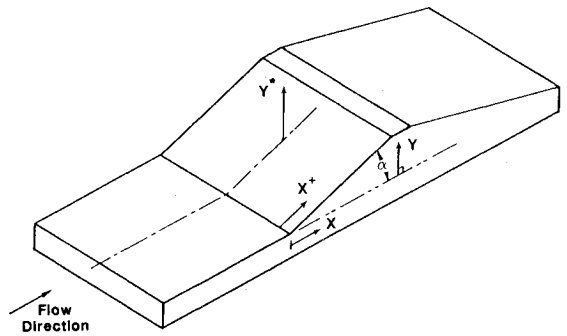

Fig. 1 Compression corner coordinate system.

Measurement Techniques

The primary measurement tool used in this investigation was a two-color laser Doppler velocimeter system. This system was used to obtain two-component mean velocity and turbulent property measurements in both the upstream and redeveloping downstream boundary layers within the five compression corner flowfields. In addition to the LDV measurements, surface static pressure measurements, surface streak pattern measurements, and high-speed schlieren photographs were also taken. The pressure measurements were used to determine the location of the beginning of the interaction, and to ensure that the ramp models were long enough to achieve a complete pressure rise. The surface streak patterns were used to check for flowfield three-dimensionality, to determine the existence of separation, and to determine the separation and reattachment locations. The schlieren photographs were used to map the flowfield and to look for any gross flowfield unsteadiness.

The LDV system used in this investigation was a two-color, two-component system utilizing optical and electronic components manufactured by Thermal Systems Inc. (TSI). A Spectra-Physics 5-W argon-ion laser operating in the multiline mode produced the necessary laser light. The beam from the laser was split into its principal components with a dispersion prism, and the green beam, with a wavelength of 514.5 nm, and the blue beam, with a wavelength of 488 nm, were used by the system. Each of these two beams was reflected down the optical axis with plane surface mirrors, and split into two equal-intensity parallel beams with beam-splitting optics. One beam of each of the two sets of parallel beams was then passed through a Bragg cell in order to shift the frequency by 40 MHz. The four parallel beams were then passed through a 350-mm focal-length lens, which caused the four beams to cross at a single point. This produced the measurement volume containing the two orthogonal fringe patterns necessary for two-component velocity measurements.

The beam spacing and 350-mm lens used in this investigation produced a measurement volume diameter of approximately 0.18 mm and a measurement volume length of approximately 6 mm. The fringe spacing was approximately 8.5 μm, and the fringe velocity due to the frequency shifting was approximately 340 m/s. The laser and transmitting optics were mounted on a traversing table which could be moved manually in three directions by means of threaded rod arrangements with an accuracy of approximately 0.1 mm. In

this manner the measurement volume could be positioned at any location within the wind-tunnel test section.

The collection optics were located on the opposite side of the wind-tunnel test section, and consisted of a 250-mm focal-length lens to collect the scattered light and a dichroic mirror and filter arrangement to separate the two color signals. These optical components were oriented 10 deg off the optical axis in order to simplify alignment procedures, and to reduce the effective measurement volume length to less than 2 mm. Photomultipliers converted the scattered light signals to analog voltage signals, and TSI frequency counters were used to determine the frequencies of the signals, and to perform validation checks to remove erroneous data. The output from the counters was stored directly in the memory of a Digital Equipment Corp. PDP 11-03 minicomputer, which converted the output into velocities and stored the data on floppy disks. The data were then transferred to a Hewlett-Packard 9000 series computer for thorough analysis.

The seed particles used in this investigation consisted of silicone oil droplets which were introduced into the wind-tunnel stagnation chamber. A series of experiments was conducted with the LDV system to determine the mean particle size, in which two-component velocity measurements were made immediately downstream of the oblique shock wave generated by the 8-deg compression corner in the Mach 2.94 flowfield. The mean velocity measurements were then compared to predicted velocities of particles of various sizes in the same flowfield conditions. The results of this series of experiments indicated that the silicone oil droplets had a mean effective diameter of between 1.5 and 2. μm. Particles of this size have been shown to have a sufficient frequency response to track the large-scale velocity fluctuations that exist downstream of shock-wave/turbulent-boundary-layer interactions.[1] The effects of particle lag were seen to some extent in the mean velocity measurements in the regions immediately downstream of the oblique shock waves due to the large velocity gradients in these regions. The influence that particle lag had on the data obtained in this investigation will be discussed during the presentation of the experimental results.

LDV measurements obtained at a particular location involve inherent uncertainties due to the finite sample size. A statistical analysis can be used to determine the level of certainty which can be attained when using the mean of a finite sample size to represent an overall population mean. The statistical uncertainty involved in determining mean velocities from individual velocity measurements is a function of the sample size and the local turbulence intensity. The sample size in this investigation was increased as local turbulence intensity increased, with 1024 samples taken when the local turbulence intensity was less than 15%, 2048 samples taken when the local turbulence intensity was between 15 and 25%, 3072 samples taken when the turbulence intensity was between 25 and 30%, and 4096 samples taken when the local turbulence intensity exceeded 30%. From a statistical analysis which assumes a normal velocity distribution, the uncertainty in mean velocity was found to be less than 2% for all velocity profiles with the exception of the two profiles nearest the compression corner in the 24-deg flowfield, in which local turbulence intensities reached values greater than 100% and the statistical uncertainty in mean velocity is of the order of 3%. The statistical uncertainty in turbulence intensity can be shown to be a function of sample size only, and for the current investigation was everywhere less than 3.6%.

Mean and turbulent flow properties computed from LDV data obtained with counter-type signal processors have been shown in the literature to be affected by biasing errors, most significantly velocity biasing[13] and fringe biasing.[14] Velocity biasing results from the fact that in a turbulent flow with uniformly distributed particles, a larger volume of fluid passes through the measurement volume during periods when the velocity is higher than the mean than when the velocity is lower than the mean. Thus, a simple average of the individual velocity measurements is biased toward higher velocities. Fringe biasing results from the fact that a particle must pass through a given number of fringes within the measurement volume for its velocity to be measured. Thus, particles traveling in a direction parallel to the fringe plane are not "seen" by the LDV, and this results in a bias in favor of particles traveling perpendicular to the fringe plane. The measurements of this investigation were corrected for the effects of velocity biasing by weighting each measurement with the two-dimensional bias correction factor $1/(u^2+v^2)^{1/2}$. The extent to which the effects of velocity biasing are removed with this correction factor is uncertain, and further research into the effects of velocity biasing and the quality of the two-dimensional correction is necessary before this issue can be completely resolved. The effects of fringe biasing were significantly reduced by the frequency shifting, which caused the fringes to move in the upstream direction, and by orienting the fringes at ± 45 deg relation to the wind-tunnel floor for the upstream boundary-layer measurements, and at ± 45 deg relative to the ramp surface for the 12-, 16-, 20-, and 24-deg compression corner redeveloping boundary-layer measurements. It was not necessary to rotate the fringes at ± 45 deg relative to the 8-deg ramp surface due to the small flow angle and low turbulence intensities in this flowfield. A comparison between the two-dimensional velocity bias corrected mean velocities, and mean velocities corrected with both the velocity bias correction and a fringe bias correction based on the analysis of Buchhave[14] yielded differences of less than 2.4%, with only six measurement differences out of nearly 800 exceeding 2%. Thus the effects of fringe bias were not significant in comparison to the effects of velocity bias, and the results presented here were corrected with the velocity bias correction only.

The particle lag, statistical uncertainty, and biasing effects described above constitute the major sources of errors in this investigation. Other less significant sources of errors include alignment accuracy, inaccuracies due to counter clock resolution, and inaccuracies in the frequency shifting components. Alignment accuracy with the LDV is believed to be quite good due to the ability to project the beams over large distances and thus make accurate measurements of small angles. The largest source of alignment error is in the orientation of the two fringe planes perpendicular to each other. This alignment is done by projecting the fringes onto a grid and aligning the beam-splitting optics. Using this procedure, the fringes were aligned within 1 deg of perpendicularity, and thus the error in velocity as a result of alignment errors is of the order of 1%. The counter-clock resolution errors result from the 1-ns resolution of the clock which measures the time required for a particle to pass through eight fringes. The amount of this error is a function of velocity, and decreases from 1.2% at a velocity measurement of 630 m/s to 0.6% at a velocity of 100 m/s. Thus, this source of error is most significant in the high-velocity regions of the flowfield, in which the turbulence intensity is low and the other sources of error such as statistical uncertainty and biasing effects are at a minimum. Errors caused by the frequency shifting components include slight changes in beam angles caused by the necessary optics, and small inaccuracies in the 40-MHz shifting frequency. A comparison between measurements made with and without frequency shifting in flowfields which were similar, but not necessarily identical, indicates that these errors are of the order of 1.5%, although one point indicated a difference of 2.3%.

Experimental Results

Undisturbed Boundary Layer

Detailed boundary-layer surveys were made with the LDV system in the turbulent boundary layer which formed on the floor of the wind tunnel in the absence of the compression corner model. These surveys were made on the wind-tunnel centerline at four stations within the test section. Two-component velocity measurements were made within the boundary

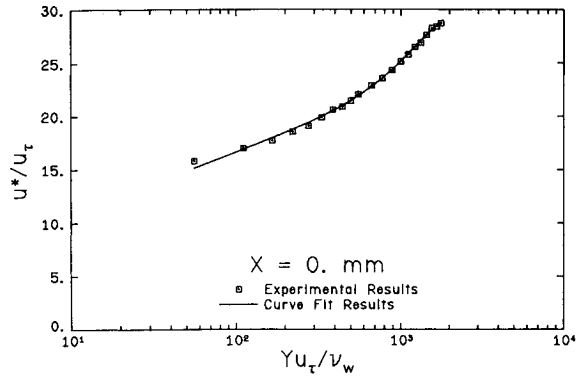

Fig. 2 Undisturbed boundary-layer profile in wall-wake law coordinates.

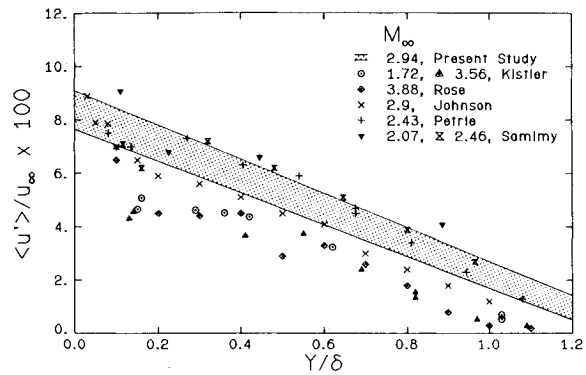

Fig. 3 Undisturbed boundary-layer turbulence intensity measurements.

layer to a point 1.5 mm ($Y/\delta_0 = 0.18$) above the wind-tunnel floor at which point blockage of the two lower laser beams began to occur. The boundary-layer surveys were completed with single-component LDV measurements down to a point 0.25 mm ($Y/\delta_0 = 0.03$) above the surface. In these measurements of the undisturbed boundary layer, frequency shifting proved unnecessary due to the relatively low turbulence intensities.

The boundary-layer thickness at $X = 0$ in the center of the test section was determined to be 8.27 mm ($u_e = 0.99u_\infty$). The displacement and momentum thicknesses were determined by numerical integration of the velocity profiles, accounting for compressibility effects, and had values of $\delta^* = 3.11$ mm and $\theta = 0.57$ mm. The Reynolds number within the test section based on boundary-layer thickness, Re_δ, was 3.1×10^5. The freestream velocity measured at $X = 0$ was within 0.2% of the velocity predicted from the measured pressure distribution.

Further details of the undisturbed boundary layer can be obtained using the transformed wall-wake law of Maise and McDonald.[15] A curve fit of the data of the current investigation to the wall-wake law can be used to obtain estimates of the wake strength parameter, Π, and the skin friction coefficient, C_f. The profile of the undisturbed boundary layer in wall-wake coordinates is shown in Fig. 2 for both the measured LDV data and the least-squares curve fit. The quantity u^* is the Van Driest generalized velocity[15] and the quantity u_τ is the friction velocity, defined as $(\tau_w/\rho_w)^{1/2}$. From this curve fit, the wake strength parameter, Π, was determined to be equal to 0.98 and the skin friction coefficient, C_f, was found to be 0.00114. Although the wake strength parameter value of 0.98 is somewhat higher than the values reported in much of the literature, Samimy[16] and Sturek and Danberg[17,18] report comparable results. The value for the skin friction coefficient agrees well with the data of Settles[2] and Sturek and Danberg.[17,18]

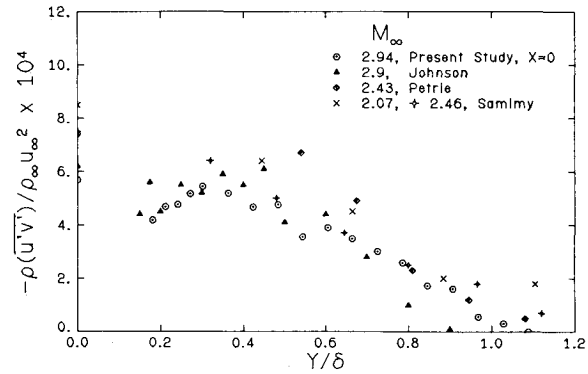

Fig. 4 Undisturbed boundary-layer shear stress measurements.

The streamwise component turbulence intensity measured with the LDV system for the undisturbed boundary layer is shown in Fig. 3. The data measured at four stations within the test section fall within a very narrow band and compare well with other experimental data. The measured turbulence intensities at the edge of the boundary layer and the freestream are probably higher than the actual levels which occur within the flowfield due to the 1 ns counter-clock resolution problem previously discussed. The turbulence intensities of this investigation are somewhat higher than the hot-wire data of Kistler[19] and Rose.[20] This difference can be attributed to the counter-clock resolution in the outer regions of the boundary layer, and possibly to difficulties in hot-wire calibration and interpretation in the lower-velocity regions of the inner boundary layer. The turbulence intensities of this investigation compare well with the LDV data of Petrie,[21] Samimy,[16] and Johnson,[22] as seen in Fig. 3.

The turbulent shear stress distribution determined from the LDV measurements within the undisturbed boundary layer at $X = 0$ is shown in Fig. 4, along with the data of Samimy,[16] Petrie,[21] and Johnson.[22] The density at each measurement location was calculated assuming adiabatic conditions within the boundary layer. Although there is a good deal of scatter in the data, the data of the current investigation agree reasonably well with those of the other three investigations. There is a tendency for the shear stress of the current investigation to reach a peak within the boundary layer and then decrease as the wall is approached. Similar shear stress behavior can be seen in data reported in other boundary-layer studies using both LDV systems[23-25] and slanted hot-wire systems.[8,9] Yanta and Lee[23] and Johnson and Rose[24] have suggested that this is the result of other turbulent shear stress terms, such as $\overline{\rho' u'v'}$, becoming significant in the lower regions of the boundary layer. However, Dimotakis, Collins, and Lang[25] suggest that this is the result of particle dynamics near solid walls which influence LDV measurements. This latter theory does not explain the decrease in shear stress near the wall that has been measured by hot-wire probes, and further study of this phenomenon is necessary.

Compression Corner Flowfields

The schlieren system was used to view the five compression corner flowfields during the initial phase of this investigation. The freestream flow was observed to be completely supersonic, and some unsteadiness was observed in the shock structures, particularly in the large ramp angle configurations, similar to the unsteadiness reported by Dolling and Murphy[26] in a 24-deg compression corner flowfield. The presence of separation near the corner was clearly visible in the schlieren photographs of the 16-, 20-, and 24-deg flowfields.

Surface streak patterns were obtained with two techniques, one using an extremely viscous oil, and a second using a kerosene-zinc oxide mixture. These techniques indicated the presence of separation in the 16-, 20-, and 24-deg compression

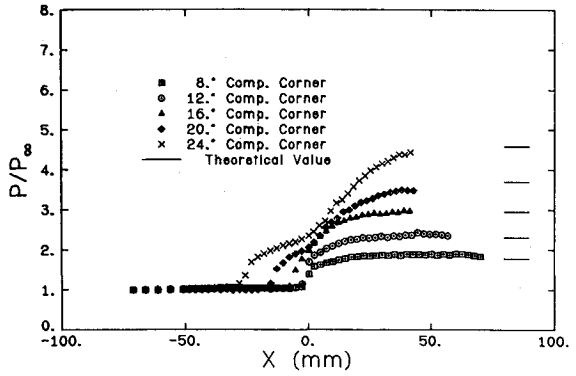

Fig. 5 Surface static pressure distributions.

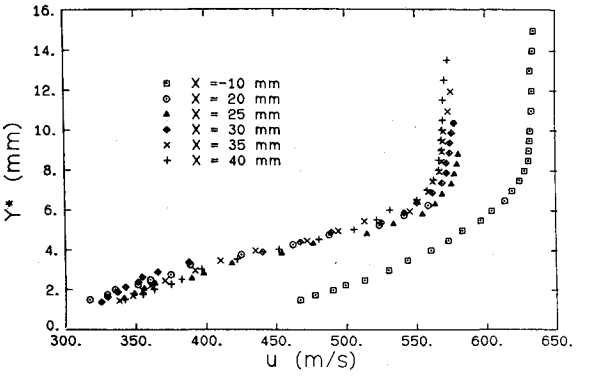

Fig. 7 Streamwise velocity profiles for the 16-deg compression corner flowfield.

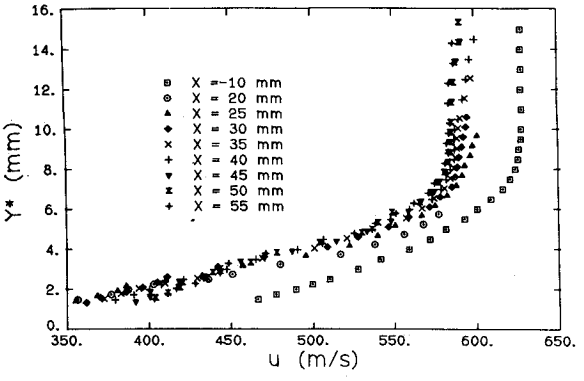

Fig. 6 Streamwise velocity profiles for the 12-deg compression corner flowfield.

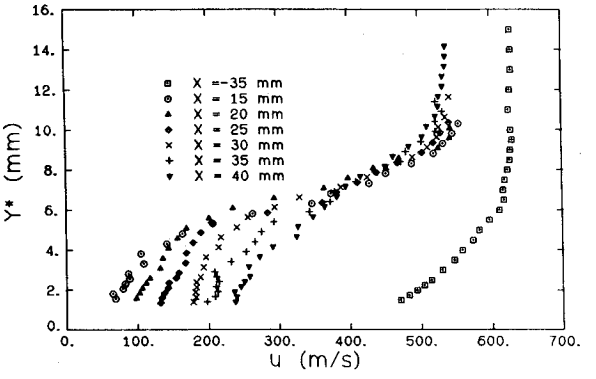

Fig. 8 Streamwise velocity profiles for the 24-deg compression corner flowfield.

corner flowfields, as well as the presence of an extremely small amount of separation in the 12-deg compression corner flowfield. This result is consistent with the results of Settles,[2] who found a very small separated region in a Mach 3, 10-deg compression corner flowfield using a similar surface flow pattern technique. From the results of these surface streak patterns, the dimensionless separation locations at the wind-tunnel centerline, X_S/δ_0, were found to be -0.12, -0.71, -1.63, and -2.95, for the 12-, 16-, 20-, and 24-deg flowfields, respectively. The dimensionless reattachment locations at the wind-tunnel centerline, X_R^+/δ_0, were found to be 0.09, 0.15, 0.52, and 1.11, for the 12-, 16-, 20-, and 24-deg flowfields, respectively. The surface streak patterns indicated some three dimensionality in the 16-, 20-, and 24-deg compression corner flowfields due to the presence of the sidewall boundary layers. As mentioned previously, this could have been significantly reduced with the use of sidewall splitter plates to reduce the effects of the wind-tunnel walls. However, the optical access necessary for the LDV measurements made the use of splitter plates impossible. In all configurations, the reattachment line was found to be very straight and free of three-dimensional effects for at least the center of 7 cm of the 10.2-cm test section width. The LDV measurements were limited to the regions upstream of separation and downstream of reattachment, and thus it is believed that the three-dimensional effects within the separated regions had a negligible effect on the LDV measurements.

The surface static pressure distributions for the five compression corners are presented in Fig. 5. The solid lines on the right side of the figure are the theoretical downstream static pressures calculated with two-dimensional oblique shock wave theory. The pressure distributions on the surface of the ramps indicate that, with the possible exception of the 24-deg configuration, the ramps were long enough to achieve full pressure recovery within the boundary layer. The 24-deg ramp was approximately 14% shorter than the critical ramp length according to the theory of Hunter and Reeves.[27] However, the reattachment point was over four boundary-layer thicknesses upstream of the end of the ramp, and the pressure near the end of the ramp was only 3% less than the theoretical value. Thus it appears that the 24-deg model was very close to the length required for full pressure recovery, and any effects of the less than optimum length were essentially negligible.

The boundary-layer velocity profiles for the 12-, 16-, and 24-deg compression corners are shown in Figs. 6, 7, and 8. The profiles for the 12- and 24-deg corners were chosen for presentation because they best illustrate the effects of large separation regions on the mean velocity profiles. The profiles for the 16-deg configuration are presented such that, with the remaining figures that will be discussed, a complete set of data for this configuration is included in this paper. The horizontal axis in these figures is the velocity component parallel to the wind-tunnel floor for the upstream boundary-layer data, and parallel to the ramp surface for the downstream data. The vertical axis is the distance from the wind-tunnel floor, or ramp surface, measured perpendicular to the upstream flow direction. The surveys were made down to a point approximately 1.5 mm above the wind-tunnel floor or ramp surface. Below this point, blockage of the two lower laser beams began to occur, making two-component measurements impossible. Single-component measurements were not made within these flowfields.

The effects of particle lag can be seen in the velocity profiles of the 12- and 16-deg configurations, in which the velocity just outside the boundary layer is relaxing toward the correct downstream value. Within the boundary layer the effects of particle lag diminish as the distance from the measurement position to the shock wave increases. The velocity in the regions nearest the wall downstream of the corners can be seen increasing with X. This results from the steeper shock wave in the lower Mach number regions of the boundary layer, which causes a larger fractional decrease in the velocity than the shock wave in the outer regions of the boundary

layer. Thus downstream of the interaction, the flow nearest the wall must accelerate as the boundary layer begins to return to an equilibrium state. This behavior was also seen in the 8-deg compression corner redeveloping boundary layer, due to the similarity of the fully attached flow and flows with only small amounts of separation.

The velocity profiles downstream of the 24-deg compression corner exhibit wake-like properties, similar to those observed by other investigators downstream of separated compression corners.[2,4,5] These wake-like profiles are the result of the redeveloping downstream boundary layer having a shear layer velocity profile as its initial condition at reattachment. The shear layer velocity profiles develop over the length of the separated region starting at the separation point of the upstream boundary layer. The velocity profiles downstream of reattachment experience a rapid "filling out," as can be seen in Fig. 8. This rapid change in the boundary-layer profiles is most likely caused by enhanced turbulent mixing, due to the formation of large-scale eddies. The decrease in the measured streamwise velocity with X, which can be seen in the outer regions of the boundary layer downstream of the 24-deg compression corner, is caused by a combination of two effects. The surface static pressure distributions, shown in Fig. 5, indicate that the pressure was still rising at the longitudinal locations where the velocity profiles shown in Fig. 8 were measured. Thus, the flow in these regions was still turning and decelerating in the final stages of the compression process. Also, the effects of particle lag may be contributing to the decrease in u with X. The rather complicated two-stage compression process caused by the presence of the separation and reattachment shock structures makes it not feasible to predict the particle lag in these regions. Thus the extent to which particle lag is contributing to this effect is uncertain.

The streamwise turbulence intensity, $\langle u' \rangle$, nondimensionalized by the freestream velocity upstream of the interaction, u_∞, is plotted for the 16-deg compression corner flowfield in Fig. 9. The turbulence intensity in the upstream boundary layer is also included for comparison. These data were chosen for presentation because they illustrate the trends of the turbulence intensity profiles seen in the data of all five flowfield configurations. In each of the redeveloping boundary layers, the level of the turbulence intensity was significantly increased by the interaction, with the amount of increase directly related to ramp angle, and thus shock strength. The turbulence intensity was found to reach a peak within the central regions of the boundary layers, and then decrease as the wall was approached, as illustrated by the data of Fig. 9. The turbulence intensity in each configuration could be seen spreading vertically with the intensity profiles becoming flatter at the downstream stations. This vertical diffusion can also be seen in the data of Ardonceau[12] downstream of a Mach 2.25 compression corner. A gradual decrease in the peak turbulence intensity accompanied this diffusion process as the boundary layer recovered from the effects of the interaction.

The maximum streamwise turbulence intensities for each measurement station are presented in Fig. 10. The maximum values plotted in this figure clearly show the increase in maximum turbulence intensity with ramp angle, and the gradual decrease of this quantity with X. Further analysis of the data from this investigation indicated that the location of the maximum turbulence intensity in each profile was also directly related to ramp angle, with the maximum values of turbulence intensity occurring further from the ramp surface for the larger shock strength interactions. A comparison of these data with the mean velocity profiles indicated that the maximum values of turbulence intensity occurred in the regions of maximum $\partial u/\partial Y^*$, due to the higher values of turbulence production in these regions of the boundary layers. It was also found that, in spite of the vertical diffusion of the turbulence within the boundary layers, the location of the maximum values remained essentially constant as the flow proceeded downstream.

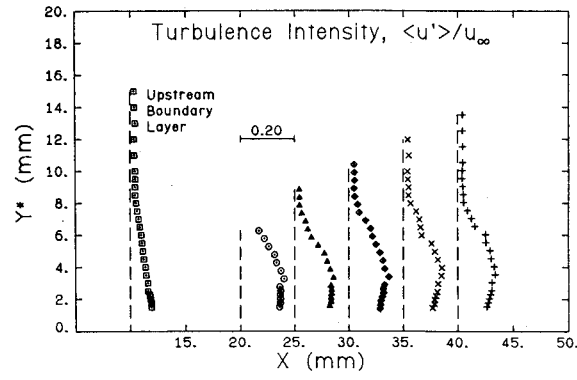

Fig. 9 Streamwise turbulence intensity profiles for the 16-deg compression corner flowfield.

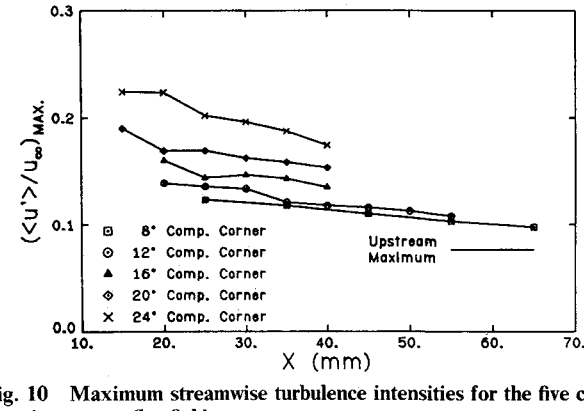

Fig. 10 Maximum streamwise turbulence intensities for the five compression corner flowfields.

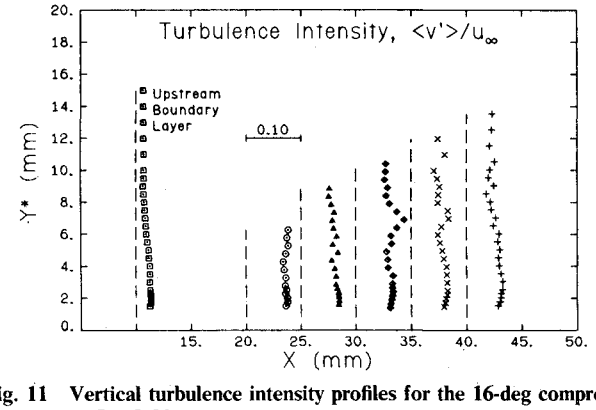

Fig. 11 Vertical turbulence intensity profiles for the 16-deg compression corner flowfield.

Vertical turbulence intensity profiles, $\langle v' \rangle / u_\infty$, are shown in Fig. 11 for the 16-deg compression corner flowfield. The data obtained in this configuration are considered representative of the data obtained for all five configurations in this investigation. It can be seen in this figure that the effect of the shock wave was to increase the vertical turbulence intensity through the interaction. A comparison of the $\langle v' \rangle$ profiles from the five configurations indicates that, similar to the $\langle u' \rangle$ data, the amount of increase in this quantity was directly related to ramp angle, and thus shock strength. However, unlike the $\langle u' \rangle$ data, the $\langle v' \rangle$ profiles show little or no dependence on the distance from the ramp surface, Y^*. There is a tendency for $\langle v' \rangle$ to reach a local maximum near the edge of the boundary layer, but this characteristic is found in only a few of the profiles measured in this investigation. It can also be seen in Fig. 11 that the vertical turbulence intensity was significantly increased in the regions outside the boundary layer. These data, in conjunction with other turbulence statis-

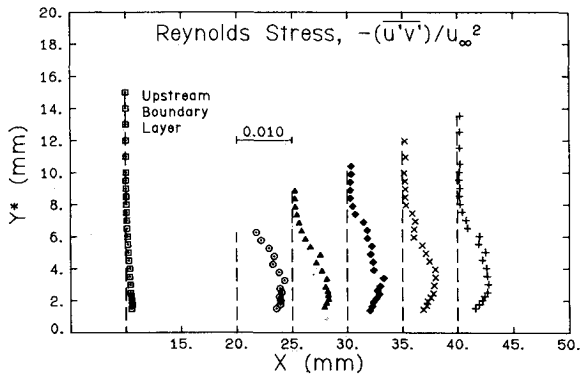

Fig. 12 Reynolds stress profiles for the 16-deg compression corner flowfield.

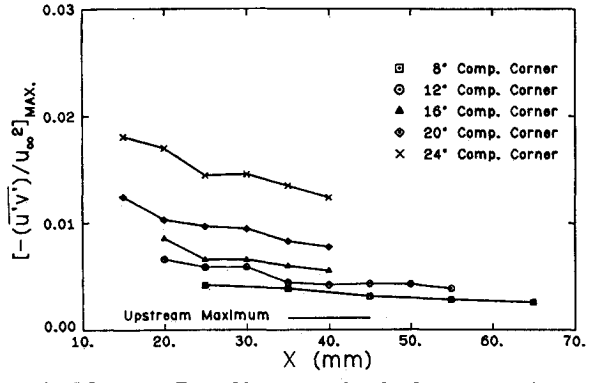

Fig. 13 Maximum Reynolds stresses for the five compression corner flowfields.

tics obtained in this investigation, such as turbulence triple products and skewness and flatness factors, indicated that there was a significant alteration of the freestream turbulence structure caused by the presence of the oblique shock wave. While it is possible that this effect is caused by particle lag, this is considered unlikely by the authors because the effects of lag diminish rapidly as the distance from the shock wave to the measuring point increases, while the large freestream values of $\langle v' \rangle$ persist to the most downstream measurement stations with very little sign of dissipation. Further studies are necessary to determine the exact nature of the effects of the oblique shock waves on the turbulence structure within the freestream flowfield.

The effects of particle lag on the mean velocity measurements can be seen in Fig. 6 in the outer regions of the boundary layer immediately downstream of the 12-deg compression corner shock wave. Some influence of this particle lag was expected in the measured turbulence intensities. In regions of significant particle lag, a false turbulence was expected due to different-sized particles decelerating at different rates, and thus producing a broad velocity histogram. However, no indications of the effects of particle lag were observed in any of the turbulence intensity profiles. The streamwise and vertical turbulence intensities in the freestream regions with significant particle lag were very similar to the values measured in the freestream regions with no significant lag. This is indicative of a relatively uniform particle size distribution, such that the false turbulence generated by the lag was insignificant in comparison to the magnitude of the turbulence within the boundary layers.

The Reynolds stress profiles for the 16-deg compression corner flowfield, nondimensionalized with u_∞^2, are presented in Fig. 12. It can be seen in this figure that the magnitude of the Reynolds stress was significantly increased by the shock wave. In all configurations the Reynolds stress reached a peak within the boundary layer and then decreased as the wall was approached. The tendency for the Reynolds stress to reach a maximum within the central regions of the boundary layer has been reported by other investigators in compression corner flowfields,[7-9] as well as in reattaching free shear layers.[16]

The maximum Reynolds stresses for each boundary-layer profile are shown in Fig. 13. Like the turbulence intensity, the maximum Reynolds stress is a strong function of ramp angle, with very large values associated with the 20- and 24-deg compression corner flowfields. These large Reynolds stresses imply the existence of large-scale eddies, which were also indicated by the rapid "filling out" of the wake-like boundary layers downstream of the 20- and 24-deg compression corner shock waves. A steady decrease in Reynolds stress with X can be seen in this figure, as the turbulence began to dissipate and diffuse through the boundary layers. The dissipation of the turbulence, however, was an extremely gradual process, and even in the weakest interaction, the ramp was of insufficient length to allow the turbulence to completely return to equilibrium conditions.

The trends in the Reynolds stresses of this investigation agree quite well with those found by researchers working with similar flowfields.[7-9] The dependency of the increase in Reynolds stress on α, the gradual decay in Reynolds stress with X downstream of the interaction, and the vertical diffusion of the Reynolds stress in the boundary layer can all be seen in the data of Muck and Smits,[8,9] for 16- and 20-deg compression corners. However, the magnitudes of $-\overline{u'v'}/u_\infty^2$ reported by these authors are significantly lower than the results of the current investigation, with the maximum values differing by factors of 2 to 4 depending on ramp angle. This discrepancy is most likely caused to a large extent by calibration problems associated with the slanted hot-wire technique used in these investigations. These authors state that the hot-wire calibration is only valid in regions in which the Mach number component normal to the wire exceeds 1.2. Taking into account the 30-deg yaw angle of the slanted hot wires, this yields a lower Mach number limit of 1.39. The local mean Mach numbers at the regions of maximum Reynolds stress in the current investigation are all below 1.39 for the 16-, 20-, and 24-deg configurations, and are close to this value for much of the data of the 8- and 12-deg configurations. In addition to these low mean Mach numbers, the high turbulence intensities in these regions indicate that the instantaneous local Mach number frequently drops far below the calibration limits, and these periods of low Mach number contribute significantly to the magnitude of $-\overline{u'v'}$. Considering these factors, it is not surprising that a large discrepancy exists between Reynolds stresses measured with slanted hot wires and those measured with two-component LDV systems in highly turbulent flowfields. An investigation in which both techniques are used to make measurements in the same flowfield would be extremely useful in resolving these discrepancies.

Conclusions

The interaction between an oblique shock wave and a turbulent boundary layer results in significant changes in both the mean and turbulent structure of the boundary-layer flowfield. The mean velocity profiles measured in this investigation indicated that the inner regions of the boundary layer were decelerated to a greater degree than the outer regions by the interaction. The profiles downstream of interactions with large amounts of separation were very wake-like in nature, with the inner regions accelerating rapidly as the boundary layers began to return to equilibrium states. Turbulence intensities and Reynolds stress values were significantly increased by the interaction, with the amount of increase directly related to ramp angle, and thus shock strength. The measured profiles of longitudinal turbulence intensity and Reynolds stress reached peak values within the central regions of the boundary layers, with the distance from the peak values to the ramp

surface also directly related to shock strength. The Reynolds stress values obtained in this investigation were significantly higher than values which have been measured in similar flowfields with slanted hot wires, and this discrepancy is believed to be due to the calibration problems associated with hot-wire systems in highly turbulent supersonic flows. The turbulent structure within the redeveloping boundary layer relaxed very gradually, such that the size limitations imposed by the wind tunnel used in this investigation prohibited the use of ramps of sufficient length to allow a complete return of the turbulent properties to upstream equilibrium values. The rapid "filling out" of the mean velocity profiles, and the large values of the measured Reynolds stresses indicated the presence of large scale turbulent structures in the flow downstream of the shock-wave/turbulent-boundary-layer interactions.

Acknowledgment

Support for this research was provided by the U.S. Army Research Office through contract monitor Dr. Robert E. Singleton under Research Contract DAAG 29-79-C-0184 and Research Contract DAAG 29-83-K-0043; and the Department of Mechanical and Industrial Engineering at the University of Illinois at Urbana-Champaign.

References

[1]Kuntz, D.W., "An Experimental Investigation of the Shock Wave-Turbulent Boundary Layer Interaction," Ph.D. Thesis, Dept. of Mechanical and Industrial Engineering, Univ. of Illinois at Urbana-Champaign, Urbana, 1985.

[2]Settles, G.S., "An Experimental Study of Compressible Turbulent Boundary Layer Separation at High Reynolds Numbers," Ph.D. Thesis, Princeton Univ., Princeton, New Jersey, 1975.

[3]Settles, G.S., Bogdonoff, S.M., and Vas, I.E., "Incipient Separation of a Supersonic Turbulent Boundary Layer at High Reynolds Numbers," *AIAA Journal*, Vol. 14, Jan. 1976, pp. 50–56.

[4]Settles, G.S., Vas, I.E., and Bogdonoff, S.M., "Details of a Shock-Separated Turbulent Boundary Layer at a Compression Corner," *AIAA Journal*, Vol. 14, Dec. 1976, pp. 1709–1715.

[5]Settles, G.S., Fitzpatrick, T.J., and Bogdonoff, S.M., "Detailed Study of Attached and Separated Compression Corner Flowfields in High Reynolds Number Supersonic Flow," *AIAA Journal*, Vol. 17, June 1979, pp. 579–585.

[6]Hayakawa, K., Smits, A.J., and Bogdonoff, S.M., "Hot-wire Investigation of an Unseparated Shock-Wave/Turbulent Boundary Layer Interaction" AIAA Paper 82-0985, June 1982.

[7]Jayaram, M. and Smits, A.J., "The Distortion of a Supersonic Turbulent Boundary Layer by Bulk Compression and Surface Curvature, " AIAA Paper 85-0299, Jan. 1985.

[8]Muck, K.C. and Smits, A.J., "The Behavior of a Compressible Turbulent Boundary Layer Under Incipient Separation Conditions," 4th Symposium on Turbulent Shear Flows, Karlsruhe, West Germany, Sept. 1983.

[9]Muck, K.C. and Smits, A.J., "Behavior of a Turbulent Boundary Layer Subjected to a Shock-Induced Separation," AIAA Paper 84-0097, Jan. 1984.

[10]Rose, W.C. and Johnson, D.A., "Turbulence in a Shock-Wave Boundary-Layer Interaction," *AIAA Journal*, Vol. 13, July 1975, pp. 884–889.

[11]Modarress, D. and Johnson, D.A., "Investigation of Turbulent Boundary-Layer Separation Using Laser Velocimetry," *AIAA Journal*, Vol. 17, July 1979, pp. 747–752.

[12]Ardonceau, P.L., "The Structure of Turbulence in a Supersonic Shock-Wave/Boundary-Layer Interaction," *AIAA Journal*, Vol. 22, Sept. 1984, pp. 1254–1262.

[13]McLaughlin, D.K. and Tiederman, W.G., "Biasing Correction for Individual Realization of Laser Anemometer Measurements in Turbulent Flows," *The Physics of Fluids*, Vol. 16, No. 12, 1973, pp. 2082–2088.

[14]Buchhave, P., "Biasing Errors in Individual Particle Measurements with the LDA-Counter Signal Processor," *Proceedings of the LDA-Symposium*, Copenhagen, Denmark, 1975, pp. 258–278.

[15]Maise, G. and McDonald, H., "Mixing Length and Kinematic Eddy Viscosity in a Compressible Boundary Layer," *AIAA Journal*, Vol. 6, Jan. 1968, pp. 73–80.

[16]Samimy, M., "An Experimental Study of Compressible Turbulent Reattaching Free Shear Layers," Ph.D. Thesis, Dept. of Mechanical and Industrial Engineering, Univ. of Illinois at Urbana-Champaign, Urbana, 1984.

[17]Sturek, W.B. and Danberg, J.E., "Supersonic Turbulent Boundary Layer in Adverse Pressure Gradient. Part I: The Experiment," *AIAA Journal*, Vol. 10, April 1972, pp. 475–480.

[18]Sturek, W.B. and Danberg, J.E., "Supersonic Turbulent Boundary Layer in Adverse Pressure Gradient. Part II: Data Analysis," *AIAA Journal*, Vol. 10, May 1972, pp. 630–635.

[19]Kistler, A.L., "Fluctuation Measurements in a Supersonic Turbulent Boundary Layer," *The Physics of Fluids*, Vol. 2, No. 3, May-June 1959, pp. 290–296.

[20]Rose, W.C., "Turbulence Measurements in a Compressible Boundary Layer," *AIAA Journal*, Vol. 12, Aug. 1974, pp. 1060–1064.

[21]Petrie, H.L., "A Study of Compressible Turbulent Free Shear Layers Using Laser Doppler Velocimetry," Ph.D. Thesis, Dept. of Mechanical and Industrial Engineering, Univ. of Illinois at Urbana-Champaign, Urbana, 1984.

[22]Johnson, D.A., "Turbulence Measurements in a Mach 2.9 Boundary Layer Using Laser Velocimetry," *AIAA Journal*, Vol. 12, May 1974, pp. 711–714.

[23]Yanta, W.J. and Lee, R.E., "Measurements of Mach 3 Turbulent Transport Properties on a Nozzle Wall," *AIAA Journal*, Vol. 14, June 1976, pp. 725–729.

[24]Johnson, D.A. and Rose, W.C., "Turbulence Measurements in Supersonic Boundary Layer Flows Using Laser Velocimetry," *Proceedings of the Second International Workshop on Laser Velocimetry*, Vol. 2, Purdue Univ., West Lafayette, IN, March 1974.

[25]Dimotakis, P.E., Collins, D.J., and Lang, D.B., "Laser Doppler Velocity Measurements in Subsonic, Transonic, and Supersonic Turbulent Boundary Layers," *Laser Velocimetry and Particle Sizing*, edited by H.D. Thompson and W.H. Stevenson, Hemisphere Publishing, New York, 1979, pp. 208–219.

[26]Dolling, D.S. and Murphy, M., "Wall Pressure Fluctuations in a Supersonic Separated Compression Ramp Flowfield," AIAA Paper 82-0986, June 1982.

[27]Hunter, Jr., L.G. and Reeves, B.L., "Results of a Strong Interaction, Wake-Like Model of Supersonic Separated and Reattaching Turbulent Flows," *AIAA Journal*, Vol. 9, April 1971, pp. 703–712.